

## Near-field characterization of guided polariton propagation and cutoff in surface plasmon waveguides

Rashid Zia,\* Jon A. Schuller, and Mark L. Brongersma

*Geballe Laboratory for Advanced Materials, Stanford University, Stanford, California 94305, USA*

(Received 22 December 2005; revised manuscript received 14 August 2006; published 25 October 2006)

We present a series of near-field experiments characterizing cutoff for the three lowest order leaky surface plasmon modes supported by Au stripes on glass substrates. These studies demonstrate that the propagation of light along surface plasmon waveguides is mediated by a discrete number of guided polariton modes as well as a continuum of radiation modes. To distinguish the contribution of the guided modes from that of the radiation continuum, a parametric study of propagation length as a function of varying stripe width is performed. Discontinuities consistent with the loss of a guided mode are observed near cutoff widths predicted by numerical simulations, and a severe decrease in propagation length is observed below cutoff for the fundamental surface plasmon mode. Contrary to previous interpretations, experimental and numerical investigations confirm that the finite propagation lengths observed along the narrowest stripes are in good agreement with an intuitive model for the radiation continuum. Furthermore, multimode interference studies provide direct evidence for multiple guided modes and support previous findings with regard to modal cutoff.

DOI: [10.1103/PhysRevB.74.165415](https://doi.org/10.1103/PhysRevB.74.165415)

PACS number(s): 73.20.Mf, 78.66.Bz, 42.79.Gn, 07.79.Fc

### I. INTRODUCTION

Surface plasmon-polaritons (SPPs) have received considerable attention for their ability to guide electromagnetic energy at optical frequencies.<sup>1-3</sup> In particular, researchers have proposed the use of surface plasmon waveguides to transport light below the diffraction limit of conventional dielectric optics.<sup>4-7</sup> The best studied surface plasmon waveguides to date have been finite width metal stripes on dielectric substrates, which have been the topic of numerous near-field microscopy studies.<sup>8-13</sup> Initial experimental results have suggested that subwavelength metal stripes may support highly confined surface plasmon modes.<sup>10,13</sup> However, recent numerical studies have shown that there is a cutoff condition for metal stripe waveguides and that no guided surface polariton modes are supported along subwavelength metal stripes.<sup>14</sup> These results suggest that guided polariton modes are insufficient to describe the observed propagation of light along metal stripe waveguides.

It is well known that a complete description of light propagation in dielectric waveguides requires a continuum of radiation modes in addition to a discrete number of guided solutions.<sup>15,16</sup> Here, we demonstrate that a similar description may be used for the propagation of light along surface plasmon waveguides. To introduce this description, we leverage a recently derived dielectric waveguide model for guided surface polaritons.<sup>17</sup> This model describes how the total internal reflection of SPPs at the edge of a metal film [as shown in Fig. 1(a)] may lead to the existence of guided surface polariton modes in a metal stripe of finite width, as shown in Fig. 1(b). Similar to the modes of a dielectric slab waveguide, SPPs along the finite width stripe must constructively interfere upon total internal reflection to form a guided mode. This interference condition establishes an eigenvalue problem with a discrete set of modal solutions. In contrast, SPPs incident below the critical angle for total internal reflection may be transmitted into the external dielectric region [as shown in Fig. 1(c)]. This transmission forms the basis for

radiation modes, and an example is shown in Fig. 1(d). Given the continuous range of possible angles below the critical condition for total internal reflection, these solutions form a continuum of radiation modes. Although the fields associated with the radiation continuum extend well beyond the finite width stripe, these solutions may contribute to the local optical field in the vicinity of the waveguide.

While previous experimental results have been mainly associated with the guided polariton modes explored by numerical studies,<sup>14,18-20</sup> it is likely that near-field measurements of the local optical intensity probe the radiation continuum as well. In the following paper, we present a series of near-field experimental studies characterizing guided polariton propagation along metal stripe surface plasmon waveguides. Using a photon scanning tunneling microscope (PSTM),<sup>21</sup> we image light propagation along finite width Au stripes on glass substrates. To distinguish the guided modes from the radiation continuum, we perform a parametric study of propagation length as a function of stripe width. Consistent with the discrete nature of the guided solutions, we observe discontinuities in the propagation length near predicted cutoff widths for the three lowest order surface plasmon modes. Furthermore, below cutoff for the fundamental guided mode, we observe propagation lengths that are consistent with a simple, width-independent model for light propagation via the radiation continuum. Cutoff widths for the higher order modes are further investigated by multimode interference studies, and all results are shown to be in good agreement with numerical simulations.

### II. EXPERIMENTAL TECHNIQUE

Similar to previous experimental studies,<sup>8-13</sup> we use a PSTM (Ref. 21) to probe the localized light intensity above metal stripe waveguides. Samples were prepared lithographically on glass substrates such that thin Au stripes protrude from extended thin film regions which serve as launchpads. To excite surface plasmon modes along the metal stripes,

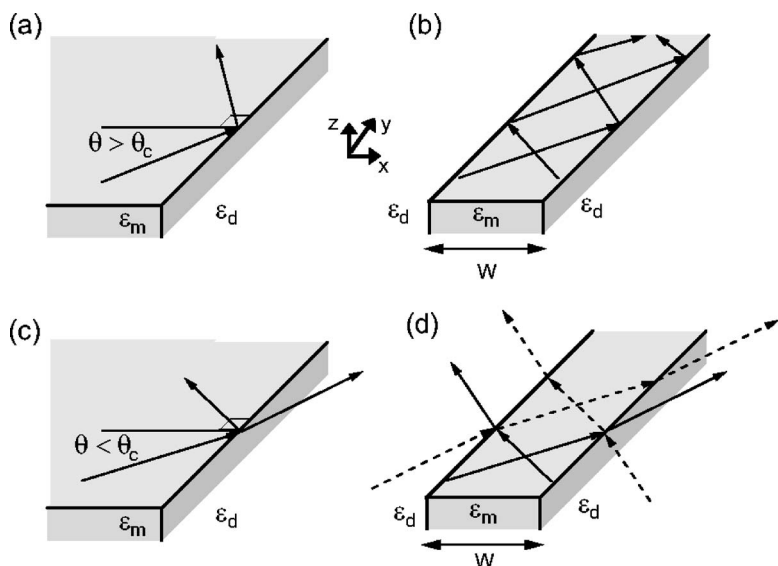


FIG. 1. Simple ray optics schematics for the modes of a metal stripe waveguide. Total internal reflection of a surface polariton wave, (a), may lead under proper interference conditions to a guided surface polariton mode, (b). Surface polariton waves may also be transmitted, (c), which necessarily leads to a radiation mode (d). Note that the radiation mode must appear to have a source outside of the waveguide to be an eigenmode of the system, as depicted by the dashed lines.

SPPs are first excited at the top air-metal interface of the extended thin film region by attenuated total reflection (ATR) in the Kretschmann configuration.<sup>22</sup> These SPPs then propagate through a tapered region to the stripe waveguides where they can excite guided polariton modes as well as radiation modes. By scanning a near-field optical probe at a constant height of 100 nm above the sample, one can map the propagation of light along the metal stripe.

A schematic of the PSTM used for this study is shown in Fig. 2. This instrument has been constructed by modifying a commercially available scanning near-field optical microscope ( $\alpha$ -SNOM; WITec GmbH; Ulm, Germany). The modified microscope is a variation on the conventional PSTM which has been used extensively to characterize SPP propagation along extended films as well as metal stripe waveguides.<sup>8-13,23,24</sup> In a conventional PSTM, SPPs are excited via ATR using prism coupling, and the local optical fields are probed by scanning a tapered fiber tip above the sample. Our PSTM operates in a similar fashion, except for three modifications. First, in the place of a prism, a partially illuminated high numerical aperture total internal reflection fluorescence (TIRF) objective (Zeiss Alpha Plan-Fluar, 100X, NA=1.45) is used to excite SPPs on the Au launchpad. Second, an aluminum-coated apertured cantilever with a 100 nm opening at the base of a hollow pyramidal tip is used as an optical near-field probe as opposed to a tapered optical fiber.<sup>25</sup> Third, instead of scanning the cantilever above a stationary sample, the sample and illumination objective are scanned on an  $x, y, z$  piezostage beneath the apertured cantilever probe. Although the presence of a near-field probe necessarily perturbs the SPP fields, we assume such as previous works on surface plasmon waveguides that these effects are small,<sup>8-13</sup> and will later show that the measured field distributions are in good agreement with numerical simulations of the SPP fields in the absence of any perturbations.

The studied metal stripe waveguides were fabricated using electron-beam lithography. In order to prevent complications arising from additional materials, the following process was developed to produce pure Au structures on glass substrates without the need for an adhesion layer such as chro-

mium or an intermediate anticharging layer such as indium tin oxide (ITO). Due to the short working distance of the TIRF objective, samples were fabricated on 150–180  $\mu\text{m}$  thick coverslips made of S1-UV grade fused silica. Cleaned substrates were spin-coated with a 100 nm thick layer of polymethyl methacrylate (PMMA, 950 K molecular weight). To prevent sample charging, a 45 Å layer of chromium was deposited on top of the cured PMMA, and following electron-beam exposure, the Cr layer was removed with a

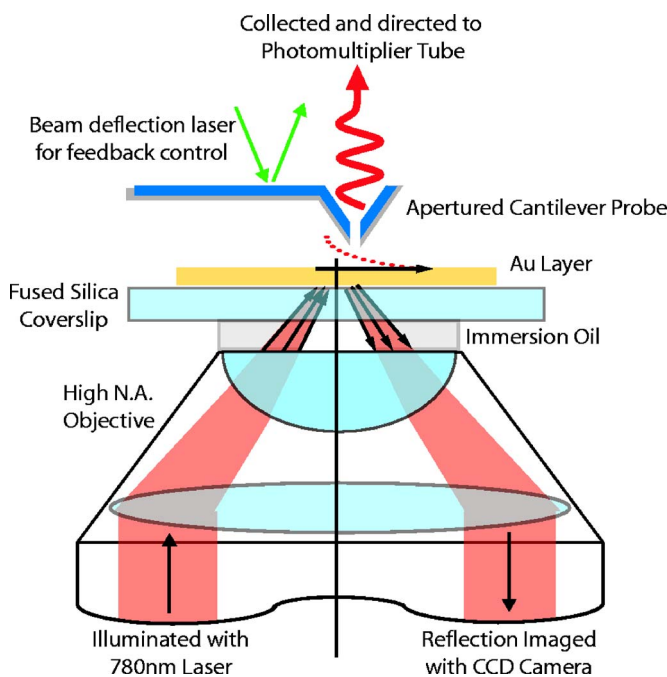


FIG. 2. (Color online) Schematic of photon scanning tunneling microscope (PSTM). A partially illuminated high numerical aperture objective is used to excite surface plasmon-polaritons along the Au-Air interface via attenuated total reflection. Light is scattered from these surface waves by an aperture cantilever probe and detected by a photomultiplier tube. Note that the sample and illumination objective are rigidly mounted to a  $x, y, z$  piezostage which is scanned below the fixed cantilever.

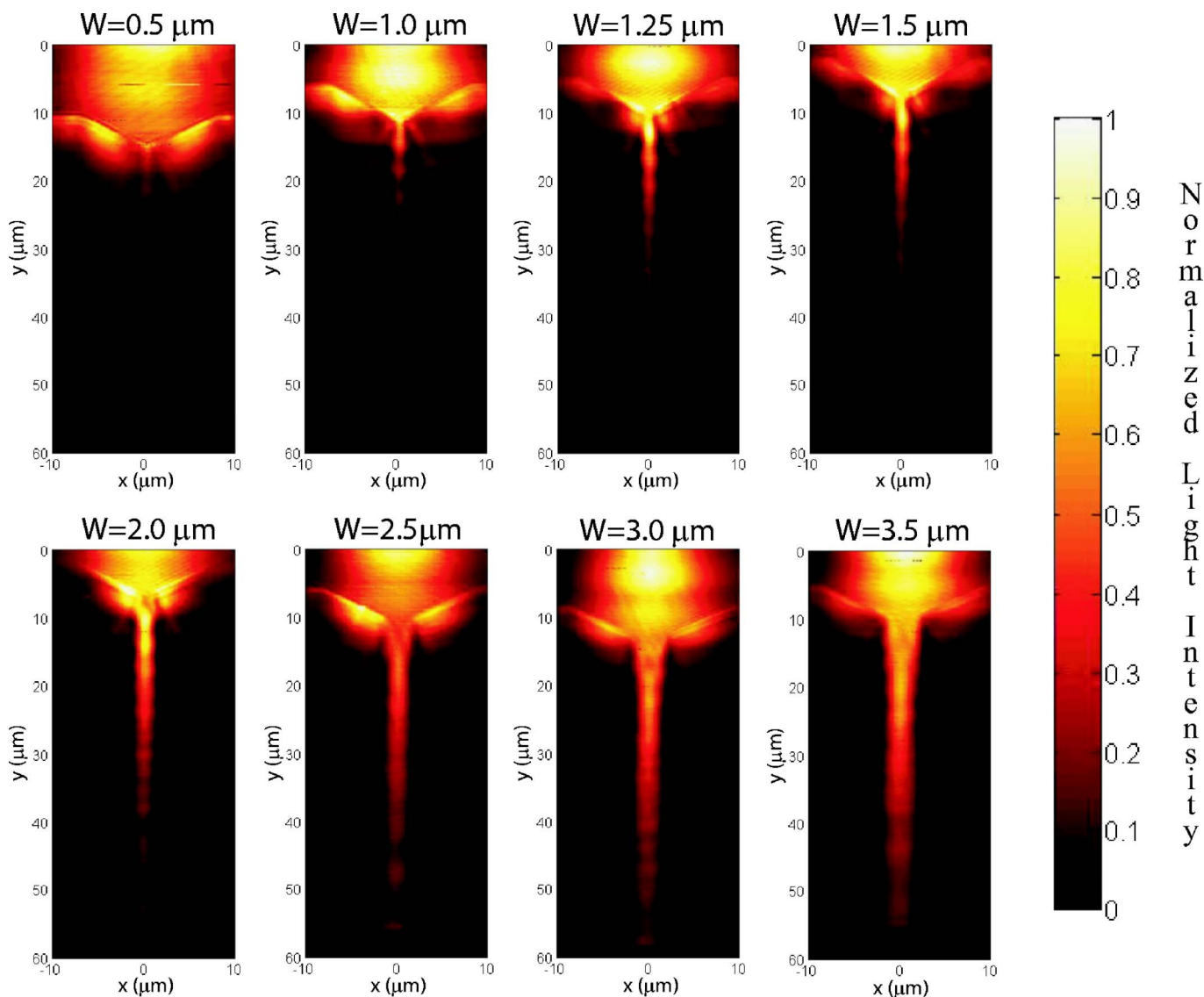


FIG. 3. (Color online) Experimental near-field images of surface plasmon propagation along varying width metal stripe waveguides ranging from  $0.5 \mu\text{m}$  to  $3.5 \mu\text{m}$ .

standard, acetic-acid based etchant. To ensure Au adhesion to the glass substrate, the developed samples were cleaned using a low power oxygen plasma ( $1-2 \text{ W/in}^2$  at 100 mTorr oxygen pressure) for 10 sec to remove residual water and hydrophilic silanol groups from the exposed glass surface. Samples were then immediately loaded into a vacuum chamber for metallization, and after reaching a base pressure below  $10^{-7}$  Torr, a 48 nm thick layer of Au was deposited via electron-beam evaporation. Fabrication was completed by standard liftoff of the remaining PMMA, and the resulting samples consisted of patterned 48 nm Au structures which directly adhered to the fused silica coverslips without any adhesion or anti-charging layers.

### III. PARAMETRIC STUDY OF PROPAGATION LENGTHS

Using the aforementioned PSTM, we have mapped the propagation of light along varying width Au stripes on glass

substrates. Fifteen different stripe widths were investigated ranging from 500 nm to  $6 \mu\text{m}$ . Figure 3 shows characteristic near-field images for the eight narrowest stripe widths. Similar to previous far-field measurements along Ag stripes,<sup>26</sup> it appears that the observed propagation length decreases as a function of decreasing stripe width. This general behavior is in good agreement with previous numerical solutions for the leaky surface plasmon modes supported by the top air-metal interface of Au stripe waveguides.<sup>14</sup> However, we can anticipate additional features in this study of propagation lengths that may distinguish guided polariton propagation by its discrete nature. In particular, a metal stripe waveguide can support a finite number of guided modes. While wide stripes may support multiple guided modes, narrower stripes may support none. In the following sections, we will show how these finite variations in mode number may be used to distinguish the discrete guided modes from the radiation continuum.

### A. Discrete nature of the guided modes

To quantify the propagation length, previous studies have commonly fit observed intensity profiles to a single decaying exponential (i.e.,  $|E|^2 \approx Ae^{-y/L} + c$ , where  $y$  denotes position along the direction of propagation,  $L$  is the  $1/e$  decay length for intensity, and  $c$  is an offset constant generally associated with background noise). Such analysis provides a qualitatively useful measure of propagation length, but the single exponential decay is an imprecise description when multiple modes are excited. As we vary the stripe width, we anticipate this inaccuracy will be most noticeable in regions where there is a transition in the number of allowed modes. In the context of waveguide theory, the electric field in a region supporting  $N$  number of guided modes may be described by the following expression:

$$\begin{aligned} \bar{E}(x, y, z) = & \sum_{n=1}^N a_n \bar{\psi}_n(x, z) e^{i(\beta_n + i\alpha_n)y} \\ & + \int_0^{+\infty} \int_0^{k_0} b_{k', k''} \bar{\psi}_{k', k''}(x, z) e^{i(k' + ik'')y} dk' dk'', \end{aligned} \quad (1)$$

where the summation and integral terms denote the contribution of the guided modes and the radiation continuum, respectively.<sup>27</sup> Each guided [radiation] mode is described by an amplitude coefficient  $a_n$  [ $b_{k', k''}$ ], transverse mode profile  $\bar{\psi}_n(x, z)$  [ $\bar{\psi}_{k', k''}(x, z)$ ], and complex propagation constant  $(\beta_n + i\alpha_n)$  [ $(k' + ik'')$ ]. Note that the summation term in Eq. (1) reflects the discrete nature of the guided polariton modes. Ignoring for the time being the contribution of the radiation continuum, we may recognize how this discrete nature influences the relationship between the physical decay constants ( $\alpha_n$ ) and the phenomenological propagation length ( $L$ ). For the case of a single guided mode (e.g.,  $N=1$ ), the propagation length is directly related to the mode's decay constant (e.g.,  $L=1/2\alpha_1$ ). For the case of multiple modes however, the fit will depend upon the relative intensities of the supported modes, and the propagation length more closely approximates a weighted average of the decay constants. Therefore for varying stripe widths, the propagation length will reflect not only changes in the decay constants, but also changes in the number of supported modes. As cutoff of a guided mode may dramatically alter a weighted average of the decay constants, we may anticipate discontinuities in the observed propagation length as a function of stripe width.

While discontinuities were not reported in previous far-field measurements,<sup>26</sup> the enhanced spatial resolution offered by near-field techniques has allowed us to observe such behavior. To calculate propagation lengths from the near-field images, we have integrated the light intensity along the width of each stripe and fit the resulting curve with a simple exponential decay, as follows:

$$\int_{-W/2}^{W/2} |E(x, y, z = h_0)|^2 dx \approx Ae^{-(y)/L} + c. \quad (2)$$

The integration here serves to average the light intensity along the stripe width.<sup>28</sup> Figure 4 shows the fit propagation

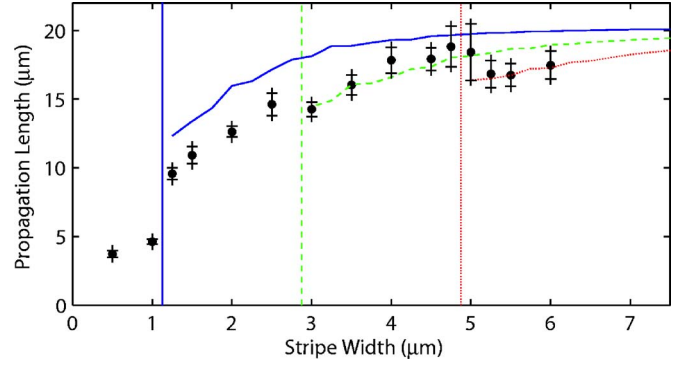


FIG. 4. (Color online) Surface plasmon propagation length as a function of stripe width at 780 nm for Au stripes on glass substrates. Circular markers denote experimental data with error bars determined by 95% tolerance intervals. The solid, dashed, and dotted curves show the calculated decay behavior for the three lowest order leaky surface plasmon modes supported by these stripes, and the associated vertical lines denote the predicted cutoff widths for these mode. Note that numerical solutions were obtained using the full-vectorial finite-difference method described in Ref. 14 for 48 nm thick Au stripes ( $\epsilon_{\text{Au}} = -24.13 + 1.725i$ ) (Ref. 29) on a glass substrate ( $\epsilon_{\text{glass}} = 2.25$ ).

length ( $L$ ) as a function of stripe width ( $W$ ). Using the full-vectorial finite difference method described previously in Ref. 14, we have also solved for leaky surface plasmon modes supported by these stripes. Alongside the experimental data, we plot the calculated decay behavior for the three lowest order surface plasmon modes. Vertical lines have been used to denote the calculated cutoff widths for the first, second, and third order modes near 1.25  $\mu\text{m}$ , 3  $\mu\text{m}$ , and 5  $\mu\text{m}$ , respectively. Note that for wider stripes (i.e.,  $W \geq 3 \mu\text{m}$ ), the observed propagation length falls within the range of values predicted by these numerical simulations. For these stripe widths, we also observe the expected discontinuities near cutoff for the higher order guided modes. While the propagation length tends to decrease with decreasing stripe width, there are two increases that oppose this trend. The propagation lengths for stripe widths between 4  $\mu\text{m}$  and 5  $\mu\text{m}$  are higher than those for wider stripes, and the propagation length increases slightly as stripe widths are reduced from 3  $\mu\text{m}$  to 2.5  $\mu\text{m}$ . These increases are consistent with cutoff for the lossier third and second order surface plasmon modes, respectively. As higher order modes are cutoff, the observed propagation length increasingly reflects the lower loss fundamental mode. Below the predicted cutoff of the fundamental guided mode, we observe a severe discontinuity. As stripe widths are reduced from 1.25  $\mu\text{m}$  to 1  $\mu\text{m}$ , the propagation length drops significantly from 9.6  $\mu\text{m}$  to 4.8  $\mu\text{m}$ . Unlike cutoff for the higher order modes where there still exist lower order modes with reduced losses, it is not surprising that cutoff of the fundamental guided mode results in a severe decrease in propagation length. This third discontinuity again reflects the discrete nature of the guided solutions, but also represents a transition to a new regime in which there are no guided modes at all.

### B. Contribution of the radiation continuum

Below the predicted cutoff width for the fundamental surface plasmon mode, it is not surprising that we continue to

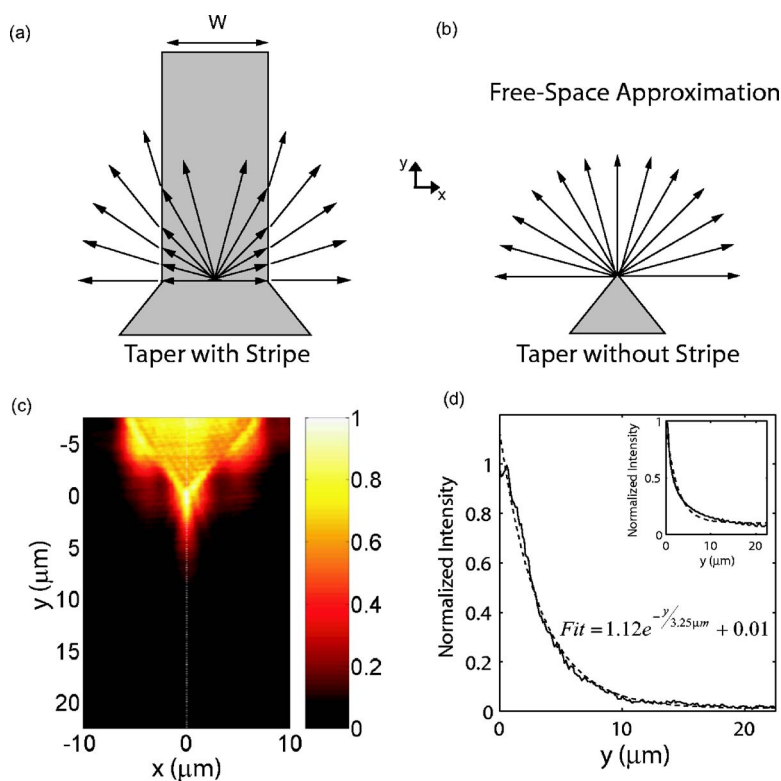


FIG. 5. (Color online) Characterization of the radiation modes using the free-space approximation: (a) the radiation modes excited at the input of a metal stripe waveguide may be modeled to first order by (b) the free-space modes excited at the end of tapered launch-pad. Even without a stripe, the experimental near-field image at the end of taper (c) appears to show light propagation along the  $y$  axis, and (d) a cross section along the dashed line can be well fit to an exponential decay. The fit propagation length ( $3.25 \mu\text{m}$ ) is in good agreement with the propagation length predicted by numerical simulations of scattered light above an extended edge discontinuity ( $2.6 \mu\text{m}$ ) as shown in the inset.

observe finite propagation lengths. The lack of guided modes along narrow stripes does not imply that light cannot propagate nor that propagation cannot be observed. Even in the absence of a metal stripe (i.e., the limiting case of infinitesimal stripe width), the termination of the tapered launchpad presents a discontinuity which should scatter SPPs into free-space radiation,<sup>30</sup> and this scattered light may be detected by our PSTM at short distances from the launchpad edge. Despite experimental differences with previous near-field studies, it is interesting to note that the observed propagation lengths for narrow stripes (i.e.,  $W \leq 1 \mu\text{m}$ ) in Fig. 4 are comparable to previous reports for subwavelength stripes.<sup>10,13</sup> Given the presence of distinctive interference patterns with subwavelength periodicities,<sup>10</sup> previous studies attributed the observed propagation lengths along narrow metal stripes to guided polariton modes. However, we suggest an alternative physical interpretation. By leveraging an intuitive physical model, we will demonstrate that the finite propagation lengths which we have observed for narrow stripes are consistent with both experimental and numerical models for the contribution of the radiation continuum.

In the context of modal theory, all nonguided pathways are described by the integral term for the radiation continuum in Eq. (1). As it is impractical to explicitly derive the amplitude coefficients, transverse mode profiles and propagation constants for all of the radiation modes, we recall the simple physical model presented in Fig. 1. In this model, the radiation modes may be decomposed into SPPs propagating along the metal stripe at variety of angles below the critical condition for total internal reflection. In the lateral direction, these SPPs are confined to the metal stripe by a small effective index gradient ( $k_{\text{spp}} = 1.022k_0$ ;  $n_{\text{eff}} = 1.022$ ).<sup>17</sup> Thus, as shown in Fig. 5(a), these SPPs can radiate laterally from the

stripe by coupling to homogenous waves in the surrounding dielectric region. Although the precise modes will depend upon the boundary conditions imposed by the stripe's edges, the resulting radiation pattern can be modeled by means of the free-space approximation.<sup>31</sup> For weakly guided dielectric structures, the radiation modes are often described as perturbations from the free-space modes within a uniform dielectric cladding.<sup>32</sup> In this manner, the radiation modes excited at the input of a metal stripe can be modeled by the light scattered into free-space from the terminated taper shown in Fig. 5(b). In Fig. 5(c), we present a near-field image of light scattered from a terminated taper, and despite the absence of a stripe, the light intensity appears to have lateral definition. To compare this model case for the radiation modes with the observed propagation along metal stripes, the cross-section shown in Fig. 5(d) has been fit to an exponential decay. The resulting propagation length of  $3.25 \mu\text{m}$  is in good agreement with the lengths observed for our two narrowest stripes. We further check the validity of the model against a numerical solution based on vector diffraction theory.<sup>30,33</sup> Using the normal mode analysis outlined in Ref. 32, we have solved for the scattered fields from an extended edge discontinuity. The calculated intensity decay is plotted in the inset of Fig. 5(d) alongside a fit exponential decay function with a propagation length of  $2.6 \mu\text{m}$ . Therefore, both experimental and numerical investigation of the free-space modes well approximate the finite propagation observed for narrow stripes, and this agreement suggests that radiation modes rather than guided modes account for the observed propagation along subwavelength stripes. Accordingly, we can conclude that a complete description of the measured near-field intensity along metal stripe waveguides requires both the discrete guided solutions as well as the continuum of radiation modes.

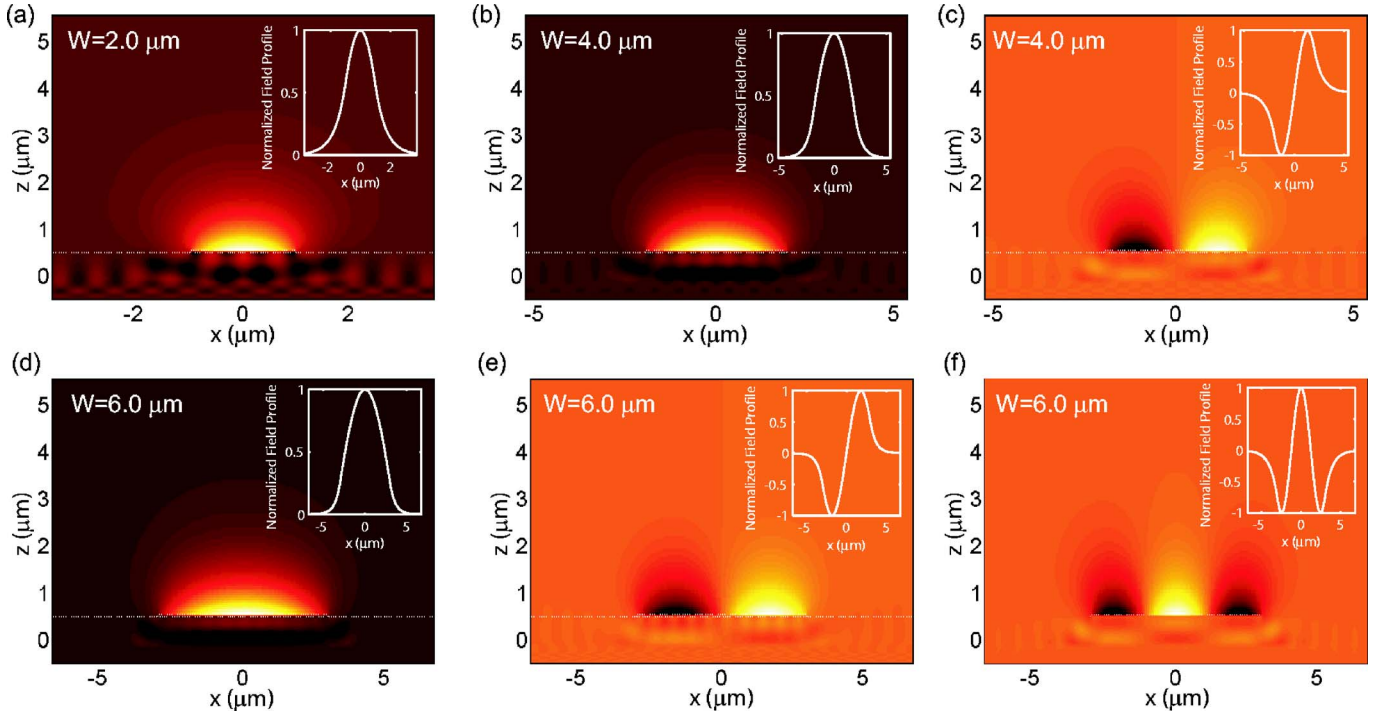


FIG. 6. (Color online) Simulated field profiles for the leaky surface plasmon modes supported by 2, 4, and 6  $\mu\text{m}$  Au stripe waveguides using the full-vectorial finite-difference method described in Ref. 14 ( $\epsilon_{\text{Au}} = -24.13 + 1.725i$  for  $\lambda = 780$  nm) (Ref. 29). Insets depict the lateral mode profiles predicted by equivalent dielectric slab waveguides as outlined in Ref. 17. The core index of the dielectric slabs was determined by the effective index of the leaky SPP mode supported along an infinitely wide 48 nm thin Au film on a glass substrate ( $n_{\text{eff}} = k_{\text{spp}}/k_0 = 1.022 + 0.003i$ , calculated using the reflection pole method) (Ref. 37).

#### IV. MULTIMODE INTERFERENCE STUDIES

In addition to distinct decay constants ( $\alpha_n$ ), each guided polariton mode is described by a unique transverse mode profile ( $\tilde{\psi}_n(x, z)$ ) and phase constant ( $\beta_n$ ). By leveraging lateral symmetries associated with the mode profiles, we have performed a parametric study of multimode interference for varying width stripes. Multimode interference is commonly exploited in the design of couplers and dividers for applications in integrated optics.<sup>34</sup> In the present context though, multimode interference may also be used to characterize the modes supported by a complex waveguide structure.<sup>35</sup>

Figure 6 shows the simulated mode profiles for the leaky surface plasmon modes supported by three varying width Au stripe waveguides. While the 2  $\mu\text{m}$  wide stripe supports only a single mode with even lateral symmetry, the wider 4  $\mu\text{m}$  and 6  $\mu\text{m}$  stripes also support a second order mode with an odd lateral symmetry. Note that the phase constant associated with this higher order mode is smaller than that of the fundamental mode, and thus, if both modes are excited simultaneously, one observes a beating in the propagation direction. To demonstrate this interference, we can excite a 4  $\mu\text{m}$  wide waveguide using a single mode 2  $\mu\text{m}$  input stripe. When the input stripe is centered with respect to the larger waveguide as shown in Fig. 7(a), we primarily excite the fundamental mode. However, when the input stripe is fabricated off-center with respect to the larger waveguide as shown in Fig. 7(b), both supported modes are excited. As evidenced by the lateral cross-sections of Fig. 7(d), there is a clear shift in the

transverse intensity profile as light propagates down the stripe. Near the input region, the lateral profile shows a single peak to the right of the dashed centerline; this profile is consistent with a superposition of the even first order mode and the odd second order mode. Further down the stripe though, the intensity of this initial peak diminishes, and an additional peak to the left of the centerline emerges. At the end of the 35  $\mu\text{m}$  long stripe, it appears that the optical intensity has switched to the other side of the 4  $\mu\text{m}$  waveguide. This lateral transition is consistent with a  $\pi$  phase shift in the relative phases for the first and second order modes, and the length scale for this transition is in good agreement with the beat length predicted by numerical simulations (i.e.,  $\pi/(\beta_1 - \beta_2) \approx 38$   $\mu\text{m}$ ).

For wider stripes, a third order leaky surface plasmon mode may also be supported. As shown in Fig. 6(f), this mode has three lateral intensity peaks in the dominant  $H_x$  field profile and an even lateral symmetry. Again, we may exploit the parity difference to demonstrate multimode interference. Similar to the previous case shown in Fig. 7(a), we use a centered 2  $\mu\text{m}$  wide stripe as the input for a larger waveguide to minimize excitation of the second order odd mode. In Fig. 8(a), we can observe multimode interference as the excited 6  $\mu\text{m}$  stripe supports two even surface plasmon modes, a fundamental mode with a single lateral peak as well as the third order with three peaks. Near the stripe input, the relative phase of the two modes is such that they interfere to form a single peak at the stripe center. With propagation though, a relative phase shift is incurred such that after propagating 30  $\mu\text{m}$  there is a local minima along the center

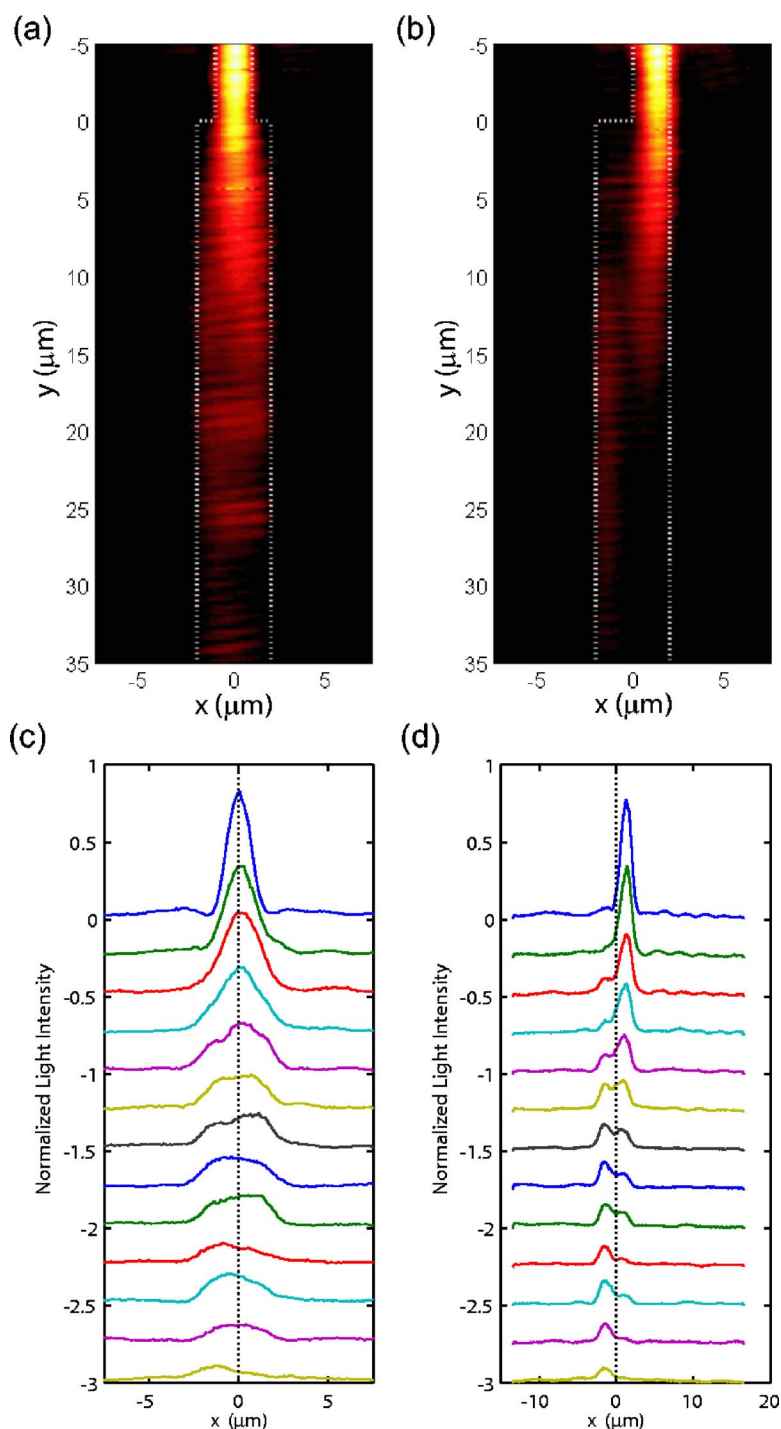


FIG. 7. (Color online) Experimental demonstration of multimode interference between the two guided modes supported by a  $4 \mu\text{m}$  wide Au stripe as excited by a  $2 \mu\text{m}$  wide input stripe. The dashed white lines indicate the outline of the Au structures. Frames (a) and (b) show near-field images acquired for symmetric and asymmetric alignment of the input stripe, respectively. Frames (c) and (d) show cross sections of the data shown in (a) and (b), respectively. Initial cross sections show the intensity above the input stripe (acquired at  $y=-1 \mu\text{m}$ ), and subsequent cross sections are taken at  $2.5 \mu\text{m}$  intervals (beginning with  $y=-2.5 \mu\text{m}$ ) and offset by  $-0.25$  increments.

of the stripe between two lateral peaks. Again, the observed beat length is in good agreement with the value predicted by full-vectorial simulations of the guided polariton modes (i.e.,  $\pi/(\beta_1 - \beta_3) \approx 29 \mu\text{m}$ ). Although the leaky nature of the guided polariton modes does not allow for simple normalization, we can leverage the dielectric waveguide model from Ref. 17 to calculate approximate lateral mode profiles for use in simple beam propagation calculations.<sup>36</sup> The observed near-field intensity in Fig. 8(a) is well modeled by multimode interference of the equivalent dielectric structure as shown in Fig. 8(b).

Accordingly, the combined experimental and numerical results shown in Figs. 6–8 unambiguously demonstrate the existence of higher order surface plasmon modes. To further support our previous findings with respect to guided mode cutoff, we have performed parametric studies of multimode interference along varying width metal stripe waveguides.

#### A. Cutoff for the odd second order mode

To investigate cutoff for the second order surface plasmon mode, waveguides ranging in width ( $W$ ) from

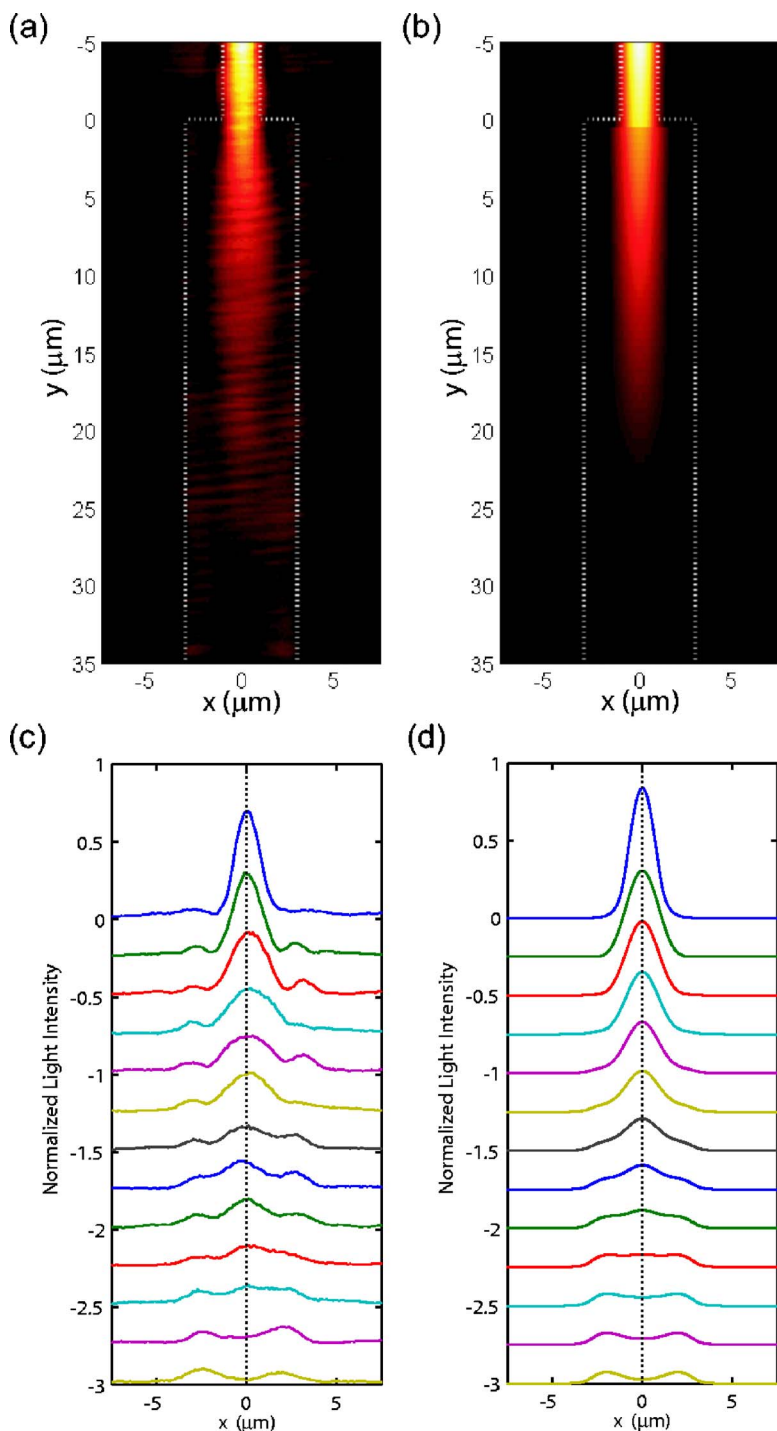


FIG. 8. (Color online) Demonstration of multimode interference between the two guided modes supported by a 6  $\mu\text{m}$  wide Au stripe: (a) experimental near-field image; (b) simulated near-field intensity for an equivalent dielectric waveguide system calculated for the approximate modes shown in the insets of Figs. 6(a), 6(d), and 6(f). The dashed white lines indicate the outline of the Au structures. Frames (c) and (d) show cross sections of the data shown in (a) and (b), respectively. Initial cross sections show the intensity above the input stripe (acquired at  $y = -1 \mu\text{m}$ ), and subsequent cross-sections are taken at 2.5  $\mu\text{m}$  intervals (beginning with  $y = -2.5 \mu\text{m}$ ) and offset by  $-0.25$  increments.

2.5  $\mu\text{m}$  to 4  $\mu\text{m}$  were fabricated with an off-center input stripe. The width of each input stripe was set to half of the value for wider waveguide such that the left edge could be aligned along the center of the larger waveguide while the right edges were continuous. For wider stripes, such asymmetric excitation clearly excited both the even and odd parity surface plasmon modes. In Fig. 9(a), the near-field image for a 3.5  $\mu\text{m}$  stripe waveguide is shown. As with the earlier example in Fig. 7(b), there is a shift in the lateral intensity profile from one side of the waveguide to the other, and the observed beat length of approximately 28  $\mu\text{m}$  is in good agreement with numerical simulations (i.e.,  $\pi/\Delta\beta \approx 31 \mu\text{m}$ ).

For the narrower 3  $\mu\text{m}$  wide waveguide shown in Fig. 9(b), the multimode interference is more difficult to distinguish. However, from the lateral cross sections shown in Fig. 9(c), one can observe the transition from a single lateral peak to the right of the centerline near the input to a pronounced peak to the left of the centerline near the predicted beat length of 25  $\mu\text{m}$ . As the stripe width was reduced further, evidence of multimode interference was not observed. Fig. 9(c) shows an example case for a 2.5  $\mu\text{m}$  stripe. Near the input region, there is a shift in the lateral intensity as the SPP diffract onto the wider stripe, but despite some undulations in intensity, the lateral profile does not appear to shift from side

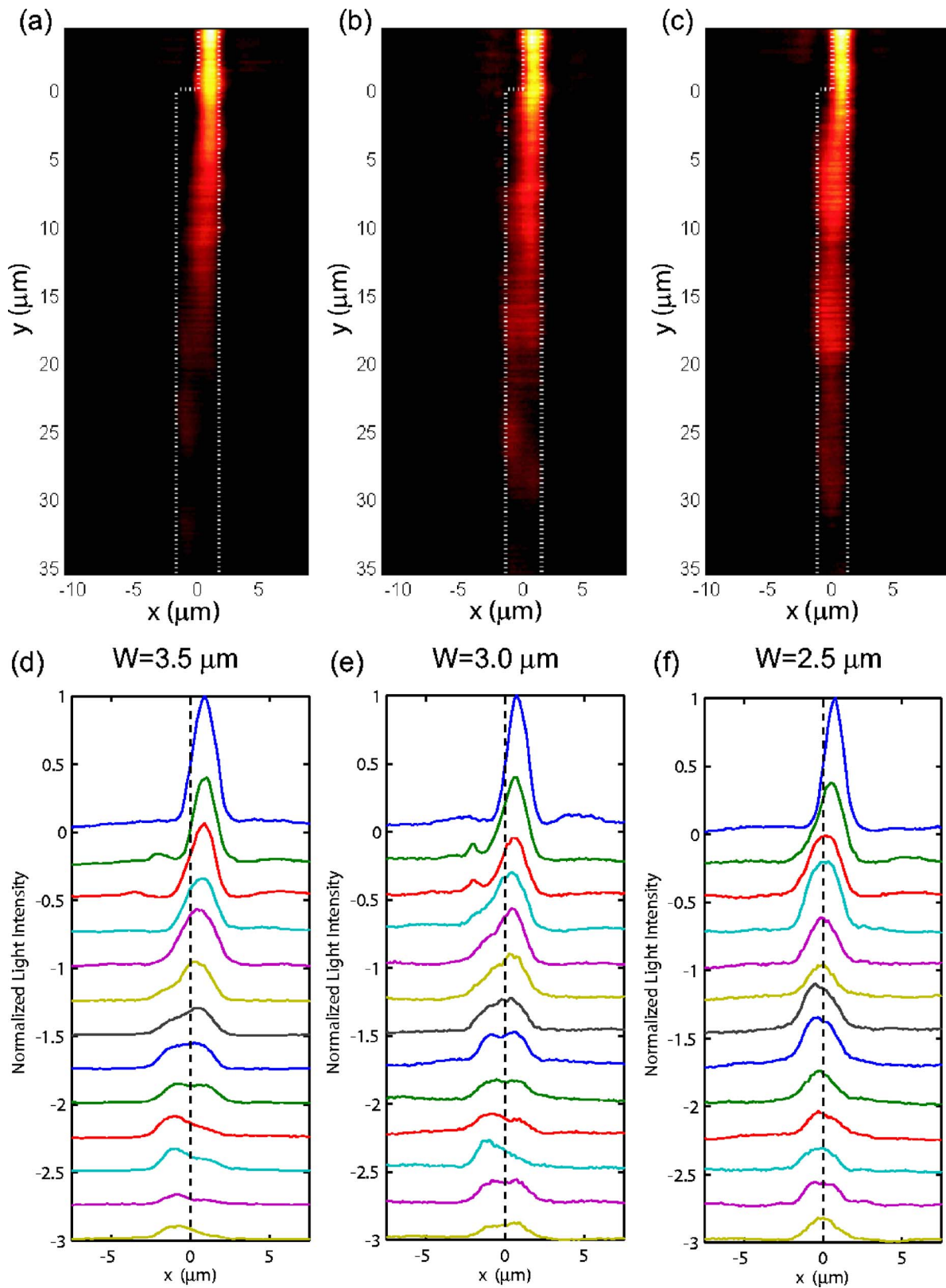


FIG. 9. (Color online) Experimental multimode interference study to investigate the cutoff width for the second order leaky surface plasmon mode. The dashed white lines indicate the outline of the Au structures. Frames (a), (b), and (c) show near-field images acquired stripe widths of  $3.5 \mu\text{m}$ ,  $3 \mu\text{m}$ , and  $2.5 \mu\text{m}$ , respectively. Frames (d), (e), and (f) show cross sections of the data shown in (a), (b), and (c), respectively. Initial cross sections show the intensity above the input stripe (acquired at  $y=-1 \mu\text{m}$ ), and subsequent cross-sections are taken at  $2.5 \mu\text{m}$  intervals (beginning with  $y=-2.5 \mu\text{m}$ ) and offset by  $-0.25$  increments.

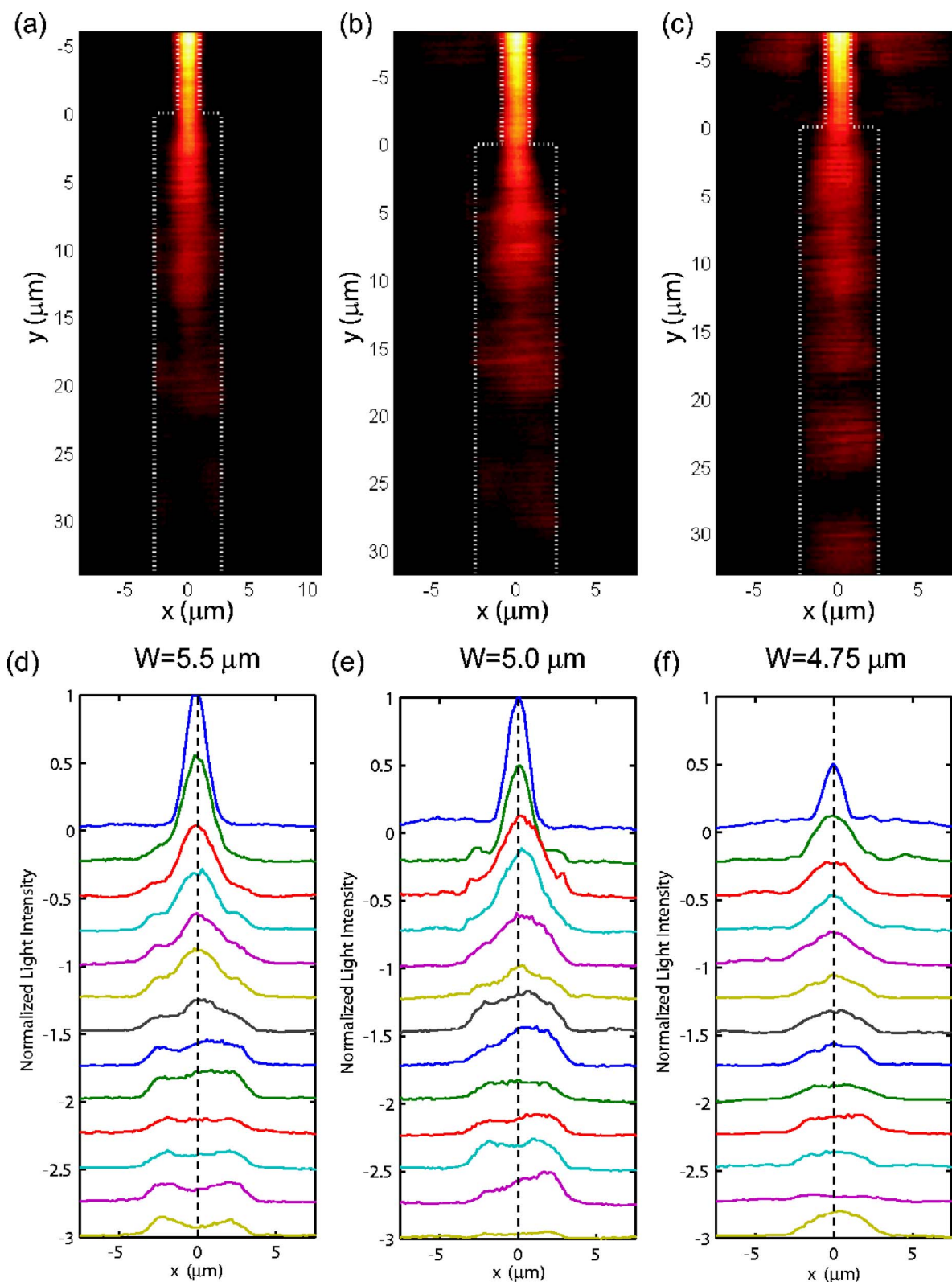


FIG. 10. (Color online) Experimental multimode interference study to investigate the cutoff width for the third order leaky surface plasmon mode. The dashed white lines indicate the outline of the Au structures. Frames (a), (b), and (c) show near-field images acquired stripe widths of  $5.5 \mu\text{m}$ ,  $5 \mu\text{m}$ , and  $4.75 \mu\text{m}$ , respectively. Frames (d), (e), and (f) show cross sections of the data shown in (a), (b), and (c), respectively. Initial cross-sections show the intensity above the input stripe (acquired at  $y = -1 \mu\text{m}$ ), and subsequent cross-sections are taken at  $2.5 \mu\text{m}$  intervals (beginning with  $y = -2.5 \mu\text{m}$ ) and offset by  $-0.25$  increments.

to side as in the earlier cases. In good agreement with the parametric propagation length study, the observation of multimode interference for the stripe widths of  $3\ \mu\text{m}$  and wider confirms the existence of a second order surface plasmon mode as predicted by numerical simulations.

### B. Cutoff for the even third order mode

To investigate cutoff for the third order surface plasmon mode, waveguides ranging in width ( $W$ ) from  $4\ \mu\text{m}$  to  $6\ \mu\text{m}$  were fabricated with a centered input stripe. The width of each input stripe was set to one third of the value for the wider waveguide in an attempt to excite the even first and third order efficiently. Similar to the studies for second order cutoff, the near-field intensity patterns were inspected for evidence of multimode interference and the observed beat lengths were compared with numerical simulations. In Fig. 10(a), the near-field image for a  $5.5\ \mu\text{m}$  stripe waveguide is shown. As with the earlier example in Fig. 8(a), the single lateral peak near the input stripe gradually diminishes with propagation as two lateral peaks emerge, and after a beat length of approximately  $30\ \mu\text{m}$  ( $\pi/\Delta\beta \approx 31\ \mu\text{m}$ ), there are two clear side lobes separated by an intensity minima. For the narrower  $5\ \mu\text{m}$  wide waveguide shown in Fig. 10(b), there appear to be two similar side peaks. In the lateral cross sections shown in Fig. 10(e), a pair of relative maxima are observed  $25\ \mu\text{m}$  down the length of the waveguide. However, this beat length is substantially longer than the value predicted by our numerical results (i.e.,  $\pi/\Delta\beta \approx 21\ \mu\text{m}$ ), and the intensity minima separating these peaks is not very pronounced. Although several similar structures were characterized, no unambiguous evidence for multimode interference was observed for  $5\ \mu\text{m}$  wide stripes. Moreover for narrower stripes, such as the  $4.75\ \mu\text{m}$  wide waveguide shown in Fig. 10(c), no clear side lobes were ever observed. Although this lack of multimode interference may result from the poor excitation efficiencies of a third order mode by the narrow input stripes, these results suggest that cutoff of the third order mode occurs near a stripe width of  $5\ \mu\text{m}$  in agreement with the presented propagation length study and numerical simulations.

## V. CONCLUSION

Through a series of experimental near-field studies, we have characterized the propagation of light along metal stripe waveguides. We demonstrated with a parametric study of propagation length that a complete modal description of metal stripe waveguides requires a discrete set of guided po-

lariton modes in addition to a continuum of radiation modes. Observed discontinuities in propagation length as a function of varying stripe width were shown to coincide with the cutoff widths predicted by numerical simulations for the leaky surface plasmon modes. A severe decrease in propagation length was observed below cutoff for the fundamental surface plasmon mode, and we demonstrated that the observed propagation lengths in this regime were consistent with a simple physical model for the radiation modes. In particular, it was shown that the observed propagation lengths for subwavelength stripes were similar to that of SPPs scattered into free-space modes at the termination of a tapered launchpad. In agreement with numerical simulations, these results suggest that previous measurements attributed to guided polariton modes along subwavelength stripes may instead have measured light propagation via the radiation continuum. To further characterize the guided polariton modes, parametric studies of multimode interference were performed. These results unambiguously confirmed the existence of higher order leaky surface plasmon modes and also supported findings with regard to the cutoff of higher order surface plasmon modes.

In light of recent results, these findings which describe modal cutoff for metal stripes also highlight the importance of alternate geometries for surface plasmon waveguides. Whereas metal stripes suffer from a decrease in propagation constant ( $\beta$ ) with narrowing width, both metallic cylinders<sup>4,38</sup> and slots<sup>39</sup> demonstrate increasing propagation constants with decreasing diameter and width respectively. Even in the presence of a high index substrate, experiments<sup>40</sup> and numerical simulations<sup>41</sup> have shown that these geometries permit waveguides of subwavelength dimension that support bound modes with subwavelength confinement. Just as metal stripe waveguides redefined the process of vertical confinement, more exotic geometries may redefine the process of transverse confinement.

## ACKNOWLEDGMENTS

The authors would like to thank Mark D. Selker for his guidance and Anu Chandran for useful discussions. Samples were patterned at the Stanford Nanofabrication Facility with the assistance of James W. Conway. This research was supported in part by a National Science Foundation Career Award (ECS-0348800), the Center for Probing the Nanoscale sponsored by the National Science Foundation (NSEC-0425897), and a Multidisciplinary University Research Initiative sponsored by the U.S. Air Force Office of Scientific Research (Grant No. F49550-04-1-0437).

\*Current address: Division of Engineering, Brown University, Providence, RI 02912. Email address: Rashid\_Zia@brown.edu

<sup>1</sup>W. L. Barnes, A. Dereux, and T. W. Ebbesen, *Nature* (London) **424**, 824 (2003).

<sup>2</sup>J. Takahara and T. Kobayashi, *Opt. Photonics News* **15**, 54 (Oct. 2004).

<sup>3</sup>R. Zia, J. A. Schuller, A. Chandran, and M. L. Brongersma, *Mater. Today* **9**, 20 (2006).

<sup>4</sup>J. Takahara, S. Yamagishi, H. Taki, A. Morimoto, and T. Kobayashi, *Opt. Lett.* **22**, 475 (1997).

<sup>5</sup>M. Quinten, A. Leitner, J. R. Krenn, and F. R. Aussenegg, *Opt. Lett.* **23**, 1331 (1998).

- <sup>6</sup>J. C. Weeber, A. Dereux, Ch. Girard, J. R. Krenn, and J. P. Goudonnet, *Phys. Rev. B* **60**, 9061 (1999).
- <sup>7</sup>M. L. Brongersma, J. W. Hartman, and H. A. Atwater, *Phys. Rev. B* **62**, R16356 (2000).
- <sup>8</sup>J. R. Krenn and J. C. Weeber, *Philos. Trans. R. Soc. London* **362**, 739 (2004).
- <sup>9</sup>J. C. Weeber, J. R. Krenn, A. Dereux, B. Lamprecht, Y. Lacroute, and J. P. Goudonnet, *Phys. Rev. B* **64**, 045411 (2001).
- <sup>10</sup>J. R. Krenn, B. Lamprecht, H. Ditlbacher, G. Schider, M. Salerno, A. Leitner, and F. R. Aussenegg, *Europhys. Lett.* **60**, 663 (2002).
- <sup>11</sup>J. C. Weeber, Y. Lacroute, and A. Dereux, *Phys. Rev. B* **68**, 115401 (2003).
- <sup>12</sup>J. C. Weeber, Y. Lacroute, A. Dereux, E. Devaux, T. Ebbesen, C. Girard, M. U. González, and A. L. Baudrion, *Phys. Rev. B* **70**, 235406 (2004).
- <sup>13</sup>L. Yin, V. K. Vlasov, J. Pearson, J. M. Hiller, J. Hua, U. Welp, D. E. Brown, and C. W. Kimball, *Nano Lett.* **5**, 1399 (2005).
- <sup>14</sup>R. Zia, M. D. Selker, and M. L. Brongersma, *Phys. Rev. B* **71**, 165431 (2005).
- <sup>15</sup>D. Marcuse, *Light Transmission Optics* (Van Nostrand Reinhold, New York, 1972).
- <sup>16</sup>D. Marcuse, *Theory of Dielectric Optical Waveguides: Second Edition* (Academic Press, Boston, 1991).
- <sup>17</sup>R. Zia, A. Chandran, and M. L. Brongersma, *Opt. Lett.* **30**, 1473 (2005).
- <sup>18</sup>P. Berini, *Phys. Rev. B* **61**, 10484 (2000).
- <sup>19</sup>P. Berini, *Phys. Rev. B* **63**, 125417 (2001).
- <sup>20</sup>S. J. Al-Bader, *IEEE J. Quantum Electron.* **40**, 325 (2004).
- <sup>21</sup>R. C. Reddick, R. J. Warmack, and T. L. Ferrell, *Phys. Rev. B* **39**, 767 (1989).
- <sup>22</sup>W. P. Chen, G. Ritchie, and E. Burstein, *Phys. Rev. Lett.* **37**, 993 (1976).
- <sup>23</sup>P. Dawson, F. de Fornel, and J. P. Goudonnet, *Phys. Rev. Lett.* **72**, 2927 (1994).
- <sup>24</sup>P. Dawson, B. A. F. Puygranier, and J. P. Goudonnet, *Phys. Rev. B* **63**, 205410 (2001).
- <sup>25</sup>C. Mihalcea, W. Scholz, S. Werner, S. Munster, E. Oesterschulze, and R. Kassing, *Appl. Phys. Lett.* **68**, 3531 (1996).
- <sup>26</sup>B. Lamprecht, J. R. Krenn, G. Schider, H. Ditlbacher, M. Salerno, N. Felidj, A. Leitner, and F. R. Aussenegg, *Appl. Phys. Lett.* **79**, 51 (2001).
- <sup>27</sup>This representation is complicated by the leaky modes supported by the stripe. In this context, some authors prefer to describe the fields in terms of a discrete number of bound and leaky modes as well as a continuum of free-space modes. [For example, see Snyder and Love, *Optical Waveguide Theory* (Chapman and Hall, New York, 1983)]. For simplicity though, we will speak of the discrete guided solutions and a continuum of radiation modes.
- <sup>28</sup>Note that this averaging also serves to minimize sensitivity to laterally dependent intensity variations, and serves to separate our present analysis from investigation of multimode interference presented in Sec. VI.
- <sup>29</sup>E. D. Palik, *Handbook of Optical Constants and Solids* (Academic, Orlando, 1985).
- <sup>30</sup>R. F. Wallis, A. A. Maradudin, and G. I. Stegeman, *Appl. Phys. Lett.* **42**, 764 (1983).
- <sup>31</sup>A. Snyder, *J. Opt. Soc. Am.* **70**, 405 (1980).
- <sup>32</sup>R. A. Sammut, *J. Opt. Soc. Am.* **72**, 1335 (1982).
- <sup>33</sup>G. I. Stegeman, A. A. Maradudin, and T. S. Rahman, *Phys. Rev. B* **23**, 2576 (1981).
- <sup>34</sup>L. B. Soldano and E. C. M. Pennings, *J. Lightwave Technol.* **13**, 615 (1995).
- <sup>35</sup>A. L. Campillo, J. W. P. Hsu, K. R. Parameswaran, and M. M. Fejer, *Opt. Lett.* **22**, 399 (2003).
- <sup>36</sup>R. Zia and M. L. Brongersma (unpublished).
- <sup>37</sup>E. Anemogiannis, E. N. Glytsis, and T. K. Gaylord, *J. Lightwave Technol.* **17**, 929 (1999).
- <sup>38</sup>C. A. Pfeiffer, E. N. Economou, and K. L. Ngai, *Phys. Rev. B* **10**, 3038 (1974).
- <sup>39</sup>R. Zia, M. D. Selker, P. B. Catrysse, and M. L. Brongersma, *J. Opt. Soc. Am. A* **21**, 2442 (2004).
- <sup>40</sup>H. Ditlbacher, A. Hohenau, D. Wagner, U. Kreibig, M. Rogers, F. Hofer, F. R. Aussenegg, and J. R. Krenn, *Phys. Rev. Lett.* **95**, 257403 (2005).
- <sup>41</sup>G. Veronis and S. Fan, *Opt. Lett.* **30**, 3359 (2005).